IEEE Access
Multidisciplinary | Rapid Review | Open Access Journal

Received 20 September 2022, accepted 8 October 2022, date of publication 13 October 2022, date of current version 20 October 2022.

Digital Object Identifier 10.1109/ACCESS.2022.3214654

RESEARCH ARTICLE

Output Characteristics of Side-Illuminated Photoconductive Semiconductor Switch Based on High Purity Semi-Insulating 4H-SiC

PYEUNG HWI CHOI[1], YONG PYO KIM[1], MIN-SEONG KIM[2], JIHEON RYU[2], (Senior Member, IEEE), SUNG-HYUN BAEK[2], SUNG-MIN HONG[1], (Senior Member, IEEE), SUNGBAE LEE[3], AND JAE-HYUNG JANG[4], (Senior Member, IEEE)

[1]School of Electrical Engineering and Computer Science, Gwangju Institute of Science and Technology, Gwangju 61005, Republic of Korea
[2]First Research and Development Institute, Agency for Defense Development, Daejeon 34186, Republic of Korea
[3]Department of Physics and Photon Science, Gwangju Institute of Science and Technology, Gwangju 61005, Republic of Korea
[4]School of Energy Engineering, Korea Institute of Energy Technology, Naju 58330, Republic of Korea

Corresponding author: Jae-Hyung Jang (jjang@kentech.ac.kr)

This work was supported in part by the Agency for Defense Development, in part by the National Research Foundation of Korea (NRF) by the Korean Government (Ministry of Science and ICT) under Grant 2017R1A2B3004049 and Grant 2022R1H1A2092527, and in part by the Korea Institute of Energy Technology (KENTECH) Research under Grant KRG2021-01-011.

ABSTRACT Photoconductive semiconductor switch (PCSS) allowing side illumination was fabricated on high purity semi-insulating (HPSI) 4H-SiC. A 532-nm pulsed laser with variable optical energy was used to trigger the PCSS. The performance of the PCSS was characterized under the two different load conditions, 50-Ω load and 0.05-Ω, with a current viewing resistor (CVR). The PCSS exhibited significantly different output characteristics for the two different loads. The equivalent resistance of the PCSS with the 50-Ω load, which was calculated from the output voltage and current, was inversely proportional to the optical energy, but the one with a 0.05-Ω load exhibited saturation behavior with the optical energy. While the times at peak output with the 50-Ω load were similar at various optical energies, the times at peak output with the 0.05-Ω load were dependent on the optical energy. Output current oscillation was also observed after the PCSS was turned off in the case of 0.05-Ω load condition. The different output characteristics for the different load resistances were analyzed using the transient response of the equivalent circuits. The PCSS exhibited a minimum on-state resistance of 0.27 Ω with the optical energy of 8 mJ and a maximum output current of 657 A at the bias voltage of 4.8 kV. The operating voltage of the PCSS was limited by surface flashover, which caused an additional output pulse following the first output pulse.

INDEX TERMS High purity semi-insulating 4H-SiC, photoconductive semiconductor switches (PCSSs), side-illumination.

I. INTRODUCTION

Photoconductive semiconductor switches (PCSSs) have attracted interest for high pulsed power devices because of their advantages, including ultrafast response, electrically isolated triggering, and negligible jitter characteristics. Single PCSS or stacked PCSSs with time synchronization have been investigated for solid-state microwave generation, including ultra-wideband (UWB), high power microwave (HPM), and dielectric wall accelerator (DWA) [1], [2], [3], [4], [5]. The ability to simultaneously generate high voltage and high current has made them attractive for applications in firing sets, ground penetrating radar (GPR), and flash x-ray generators [6], [7], [8]. PCSSs have achieved high output currents up to the kA range in non-linear or lock-on mode, where an avalanche multiplication occurs [9], [10], and in linear mode operation, where the output current reaches hundreds of amperes [11], [12], [13].

The associate editor coordinating the review of this manuscript and approving it for publication was Stanley Cheung.

The operational characteristics of PCSSs also have been investigated for high power switching with a load resistance ranging from 0.05 to 50-Ω. High power microwave pulse generators generally drive antenna so that the solid-state switches for microwave applications have been characterized with 50-Ω load impedance [2], [14], [15]. Linear transformer drivers (LTD) have driven load impedances lower than 1-Ω to maximize the circuit current output [16], [17]. To observe high current switching characteristics, a current viewing resistor (CVR) has been employed in series with the PCSS. Because the CVR has a resistance in the sub-Ω range, the on-state resistance of the PCSS is much higher than the resistance of the CVR and dominantly drives the output current. Most of the bias voltage is applied to the PCSS, and this allows the output characteristics of the PCSS under a high electric field to be investigated at a relatively lower bias voltage than one at a load resistance of 50-Ω. Conventional lateral-type GaAs-based PCSSs with gap sizes of 1.5 and 2 mm were characterized in series with a 0.1-Ω CVR [9]. When the PCSS was excited with an optical laser with a wavelength of 1064 nm and energy of 16 mJ, the PCSS switched the maximum output current of 1.5 kA at a bias voltage of 2 kV in lock-on mode, and the effect was investigated at various charging circuit capacitances. Another study on a GaAs based lateral-type PCSS operating in non-linear mode demonstrated the maximum switching current of 1.5 kA and investigated the failure mechanism of the PCSS with a 0.1-Ω CVR [10].

SiC-based PCSSs, in linear mode operation, have also been investigated for the higher hold-off voltage. A vanadium compensated semi-insulating (VCSI) 4H-SiC based PCSS employing a transparent window and silver mirror reflector was characterized with a 0.05-Ω CVR and exhibited the maximum switching current of 840 A at a bias voltage of 12 kV [18]. Another vertical PCSS based on VCSI 6H-SiC was tested with a load resistance of 20-Ω in series with a CVR and a current coil to monitor the current. To predict the operational characteristics of PCSS in linear mode operation, the PCSS resistance was modeled using the carrier density and a PSpice simulation. The simulation and experiment demonstrated high-power RF generation with a switching current of 590 A at a bias voltage of 18 kV [13].

To accurately measure the on-state resistance of a PCSS based on VCSI 4H-SiC, the impedance of the test circuit, including PCSS and a 0.0249-Ω CVR was analyzed and extracted photoconductivity of 4H-SiC substrate [19]. Another work conducted an equivalent circuit analysis for the test circuit including a load resistance of 100-Ω in series with a 0.1-Ω CVR [20]. By estimating the capacitance of the VCSI 6H-SiC based PCSS and the circuit inductance, PSpice model for PCSS was developed to accurately simulate the output waveform of the PCSS circuit triggered by double optical pulses with a time interval. To investigate the potential high frequency operation of the VCSI 4H-SiC based PCSS, both the physics modeling for the resistance and the impedance analysis of the test circuit were conducted with a 1030 nm

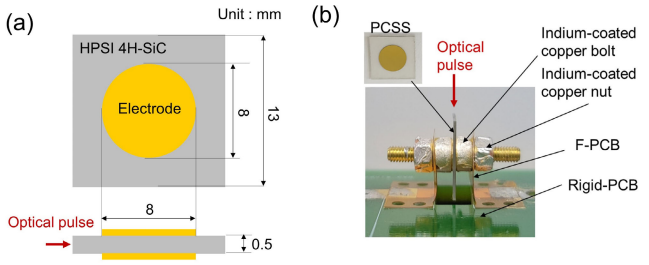

FIGURE 1. a) Schematics of vertical PCSS based on HPSI 4H-SiC. (b) Pictures of the device modules mounted with indium-coated copper bolts on a flexible printed circuit board (F-PCB).

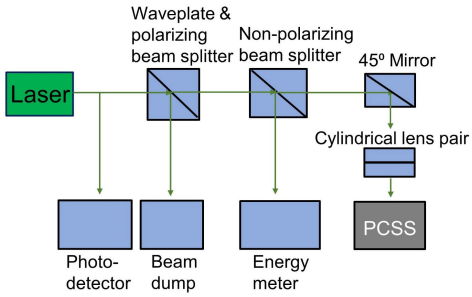

FIGURE 2. Optical trigger setup for photoconductivity test.

laser at 1 MHz repetition rate [21]. While the above studies with circuit modeling confirmed the validity of the simulation results, the detailed output characteristics and current oscillation of the PCSS have not yet been investigated.

In this work, a side-illuminated vertical PCSS based on HPSI 4H-SiC was fabricated to investigate current switching capability. The side-illuminated vertical PCSS device exhibited high optical absorption efficiency so that a low on-state resistance can be achieved at low optical excitation energy [22]. A 532-nm laser was utilized for the optical coupling of the entire volume of the vertical PCSS. The PCSS with a 0.05-Ω CVR exhibited different output characteristics compared to one with a 50-Ω load. The transient response analysis of the equivalent circuit elucidated that the minimum on-state resistance, the time at peak output, and the current oscillation phenomena are closely related to the load resistance. In addition, the maximum switching current of the PCSS and the surface flashover, which limits the PCSS operating voltage, were investigated.

II. EXPERIMENTAL SETUP

A 500-μm-thick HPSI 4H-SiC substrate with a resistivity higher than $10^7 \Omega \cdot$ cm and a micro-pipe density lower than 0.1 cm^{-2} was used to fabricate the vertical-type PCSS devices. As shown in Fig. 1(a), 8-mm-diameter circular electrodes were formed on both sides of the 1.3 $\times$ 1.3 cm^2 substrate by optical lithography, where the photoresist (AZ5214) was utilized for image reversal process and a mask aligner (M100, PRO Win) was used for optical exposure and flood exposure. Subsequently, the multilayer metallization consisting of Ni/Ti/Au (40/40/300 nm) was evaporated and lifted-off

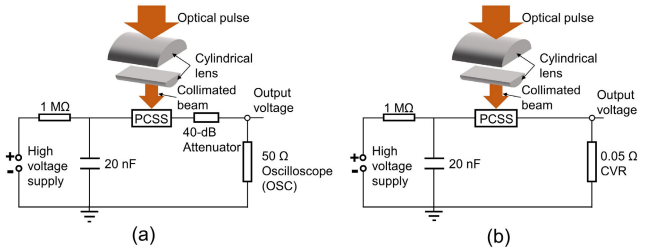

FIGURE 3. PCSS test circuit setup measured by (a) 50-Ω terminated oscilloscope (OSC) (b) 0.05-Ω current viewing resistor (CVR).

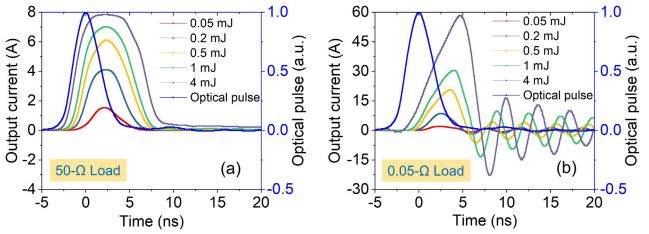

FIGURE 4. Optical pulse waveform measured with the 2-GHz Si photodetector (blue) and (a) output current waveforms of the PCSS measured by 50-Ω terminated oscilloscope with various optical energies and a bias voltage of 400 V (b) output current waveforms of the PCSS with a 0.05-Ω current viewing resistor at the bias voltage of 400 V.

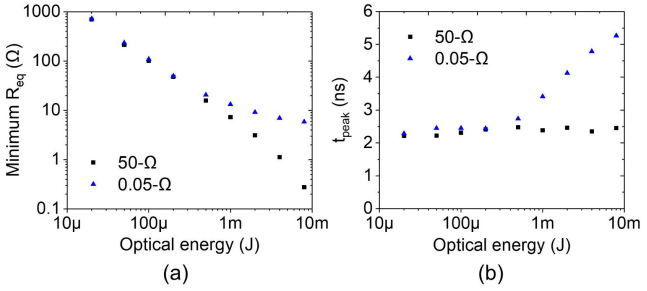

FIGURE 5. (a) Minimum equivalent resistance (R_{eq}) and (b) time to reach the peak output current (t_{peak}) measured for variable optical excitation energy. The HPSI 4H-SiC PCSS was measured using the load resistances of 50-Ω and 0.05-Ω, respectively, as a function of the optical energy at a bias voltage of 400 V.

[22]. As shown in Fig. 1(b), indium-coated copper bolts and nuts were utilized for the electrical connection to flexible PCB (F-PCBs). The F-PCBs were bent so that the device could be maintained at a right angle to the rigid-PCB.

The optical trigger setup for the PCSS device is shown in Fig. 2. A 532-nm optical pulse was generated from a Q-switched Nd:YAG laser (Quantel, Brilliant Eazy) with a beam diameter of 5.18 mm, full width at half maximum (FWHM) of 2.9 ns, and a repetition rate of 10 Hz. The optical pulse energy was varied from 20 μJ to 8 mJ using a wave plate and polarizing beam splitter cubes, and beam dump (PL 15, Newport) was utilized to absorb the waste optical energy. The optical illumination energies were measured by an energy meter (QE25LP-S-MB-QED, Gentec). The circular laser beam was changed to a collimated elliptical beam by using two cylindrical lenses with a focal length ratio of 10:1. The collimated laser beam illuminated the side facet of the device.

The optoelectronic test circuits with load resistances of 50-Ω and 0.05-Ω are shown in Figs. 3(a) and 3(b), respectively. Both circuits utilized a charging capacitor (C_c = 20 nF) and resistor (1 MΩ). When the optical pulse triggers the PCSS, the charge stored in the capacitor begins to discharge through the PCSS. As shown in Fig. 3(a), the electrical pulse is attenuated by a 40-dB coaxial attenuator (WA42-40-34, Weinschel), and then measured by a 50-Ω terminated digital phosphor oscilloscope (DPO 7254, Tektronix) with a bandwidth of 2.5 GHz. Fig. 3(b) shows the experimental setup to monitor electrical current pulse with a CVR (SBNC A-1-05, T&M Research Products), having a resistance of 0.05-Ω. The voltage drop across the CVR was measured with a 50-Ω terminated DPO. The optical pulse was measured with a 2 GHz Si photodetector (DET025AL, Thorlabs), and then was utilized as a triggering signal for the output electrical pulse measurement.

III. RESULTS AND DISCUSSION

To investigate its output characteristics, the PCSS was tested at a bias voltage of 400 V and optical energies ranging from 20 μJ to 8 mJ. Fig. 4(a) shows the waveforms of the optical trigger pulse, where the time at the peak optical power was set to 0 to use it as the timing reference, and the electrical output current of the PCSS with a load resistance of 50-Ω. The typical output pulse exhibited a Gaussian shaped waveform. It was also found that the time to reach peak output current, t_{peak}, was similar for various optical energies. The peak output current of the PCSS illuminated by the optical energy 4 mJ was 7.84 A, and the FWHM of the output pulse was 7.9 ns. The output characteristics of the same PCSS measured with the 0.05-Ω CVR are shown in Fig. 4(b). When the same optical pulse was applied to the PCSS, the peak output current was 58 A, and the FWHM of the output pulse was 4.89 ns. It was observed that the t_{peak} depended on the incident optical energy. The current pulse exhibited a steeper falling edge than the rising edge, and damping oscillation.

To qualitatively analyze the output characteristics, the equivalent resistance of the PCSS, R_{eq}, was calculated from the output voltage and current with the following equation:

$$R_{eq} = \frac{V_c - V_o}{V_o} R_L, \tag{1}$$

where V_o is the output voltage, R_L is the load resistance. V_c is capacitor voltage at time t, and can be calculated as:

$$V_c(t) = V_{bias} - \int_{-\infty}^{t} \frac{V_o(t')}{R_L C_c} dt', \tag{2}$$

where V_{bias} is the dc bias voltage applied by a high voltage supply and C_c is the charging capacitance of 20 nF.

Fig. 5(a) shows the minimum R_{eq} at various optical energies. When the PCSS was characterized with load resistances of 50-Ω and 0.05-Ω, the minimum R_{eq} were the same at optical energies lower than 0.5 mJ, however, the minimum

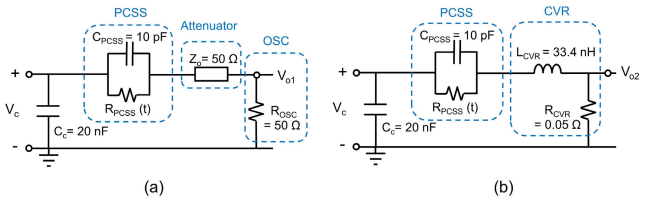

FIGURE 6. Equivalent circuits of test setups with load resistances of (a) 50-Ω (b) 0.05-Ω.

R_{eq} with the CVR showed saturating behavior at optical energies higher than 0.5 mJ. The t_{peak} values measured with 50-Ω and 0.05-Ω loads were similar at optical energies lower than 0.5 mJ, but the t_{peak} measured with the CVR increased at optical energies higher than 0.5 mJ, as shown in Fig. 5(b).

To analyze the different output characteristics of the two cases, equivalent circuit analyses were conducted. The equivalent circuits of the test circuit with the load resistances of 50-Ω and 0.05-Ω are shown in Figs. 6(a) and (b), respectively. The capacitance of the PCSS, C_{PCSS}, and inductance of the CVR, L_{CVR}, were measured to be 10 pF and 33.4 nH, respectively. In Fig. 6(a), the internal on-state resistance of the PCSS, R_{PCSS}(t), can be calculated as follows [23]:

$$R_{PCSS}(t) = \frac{V_c(t) - V_o(t)}{\frac{V_o(t)}{R_L} - I_{C,PCSS}(t)} = \frac{V_c(t) - V_o(t)}{\frac{V_o(t)}{R_L} - C_{PCSS}\left(\frac{dV_o(t)}{dt} + \frac{V_o(t)}{R_L C_c}\right)}, \quad (3)$$

where $I_{C,PCSS}(t)$ is the current along the capacitance of the PCSS.

Since the resistivity of the PCSS was determined by the optical energy, $R_{PCSS}(t)$ is identical regardless of the load resistance at the same optical energy. Then, $V_c(t)$ in Fig. 6(b) can be expressed as follows:

$$V_c(t) = V_{PCSS}(t) + V_{L,CVR}(t) + V_{R,CVR}(t) = R_{PCSS}(t)\left(I_{CVR}(t) - I_{C,PCSS}(t)\right) + L_{CVR}\frac{dI_{CVR}(t)}{dt} + I_{CVR}(t)R_{CVR}, \quad (4)$$

where $V_{L,CVR}$ and $V_{R,CVR}$ are the voltages across the inductance and resistance of the CVR, respectively. I_{CVR} is the current along the CVR. Then, $I_{C,PCSS}(t)$ can be expressed as follows:

$$I_{C,PCSS}(t) = C_{PCSS}\frac{dV_{PCSS}(t)}{dt} = C_{PCSS}\frac{d(V_c(t) - V_{L,CVR}(t) - V_{R,CVR}(t)}{dt} = -\frac{C_{PCSS}}{C_c}I_{CVR}(t) - L_{CVR}C_{PCSS}\frac{d^2I_{CVR}(t)}{dt^2} - R_{CVR}C_{PCSS}\frac{dI_{CVR}(t)}{dt} \quad (5)$$

The $R_{PCSS}(t)$ acquired with a load resistance of 50-Ω is discretized with the time interval Δt of 12.5 picoseconds, which is the sampling time during the measurement. To input

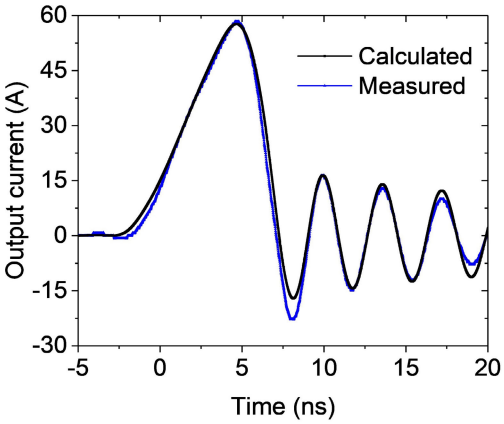

FIGURE 7. Output current waveform calculated (black) and the output current waveform measured using a 0.05-Ω CVR (blue).

the measured $R_{PCSS}(t)$ into the time domain equation, (4) was changed to the difference equation by discretizing the time with Δt and can be expressed as the following equation:

$$V_N = R_N(I_N(1 + \frac{C_{PCSS}}{C_c}) + L_{CVR}C_{PCSS}\frac{I_{N+1} - 2I_N + I_{N-1}}{(\Delta t)^2} + R_{CVR}\frac{I_{N+1} - I_{N-1}}{2\Delta t}) + L_{CVR}\frac{I_{N+1} - I_{N-1}}{2\Delta t} + I_N R_{CVR}, \quad (6)$$

where V_N is $V_c(t = t_N)$, I_N is $I_{CVR}(t = t_N)$, R_N is $R_{PCSS}(t = t_N)$, and t_N is $t_{N-1} + \Delta t$. The discrete sequence of I_{N+1} can be obtained by (7), as shown at the bottom of the next page.

Considering that V_N is capacitor voltage at t_N, the current I_N at t_N can be obtained by inserting the measured value of R_N at the optical energy of 4 mJ into (7). The waveform of I_N and transient output current waveforms, $I_{CVR}(t)$, are shown in Fig. 7, and the two waveforms are well-matched, which implies that the different output characteristics are due to the lumped components of test circuits and minimum R_{PCSS} at both load conditions were same. The $dI_{CVR}(t)/dt$, which is the derivative of the output current with respect to time, was 11 A/ns at the time of 2.3 ns, which is the average t_{peak} measured with a 50-Ω load at the optical energy of 4 mJ, so that an induced voltage of 367 V was applied to the inductance of the CVR. The induced voltage limits the output current increases with time. The dI_{CVR}(t)/dt at the optical illumination energy higher than 0.5 mJ was so high that the time to reach the peak current, t_{peak}, was different with the time required for R_{PCSS} to reach the minimum value, and t_{peak} was delayed even further as the optical energy increased.

The current oscillation was observed, as shown in Fig. 4(b). Since the current along the shunt capacitance of the PCSS is far higher than the current along the high resistance of the PCSS, the current oscillation takes place due to the series RLC circuit composed with R_{CVR}, L_{CVR}, and C_{PCSS}. The oscillation period can be calculated as follows:

$$T_{cir} = \frac{1}{f} = 2\pi\sqrt{L_{CVR}C_{PCSS}}. \quad (8)$$

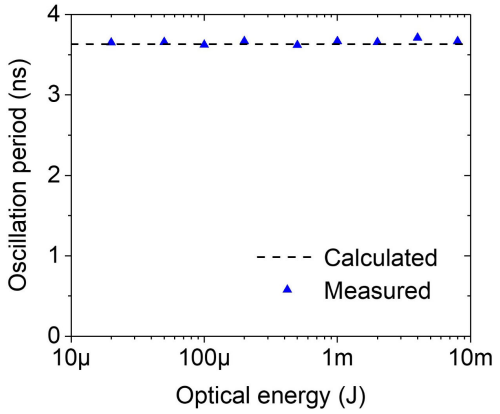

FIGURE 8. Oscillation periods calculated from the oscillation frequency of the series RLC circuit (black, dashed line), and measured (blue, triangle) with a load resistance of 0.05-Ω at a bias voltage of 400 V for various optical energies.

The calculated oscillation period was determined to be 3.63 ns. The average oscillation periods measured by the CVR at various optical energies are shown in Fig. 8. On the other hand, the test circuit with 50-Ω load has the higher load resistance and the much smaller parasitic inductance than the test circuit with CVR. With the higher damping and the lower reactance component, the current oscillation was suppressed.

To investigate the maximum switching current, the PCSS was characterized under bias voltages ranging from 100 V to 4.9 kV with a 0.05-Ω load at the optical energy of 8 mJ. The output waveforms under various bias voltages are shown in Fig. 9(a). The oscillation period at various voltages is essentially the same, but the ratio of the oscillation level at the first damping to the peak output current decreases as the bias voltage increases. As shown in Fig. 9(b), the peak output current increased linearly with bias voltage, and the maximum switching current was 657 A at a bias voltage of 4.8 kV. At a bias voltage of 4.9 kV, surface flashover, which limited the current switching capability of the PCSS, took place along the surface of the PCSS substrate, as shown in Fig. 10(a). Fig. 10(b) shows that both electrodes and the surface of the substrate were damaged due to the surface flashover. An appropriate surface passivation using a dielectric layer would be an effective way to improve the current switching performance of the side-illuminated vertical PCSS.

The performances of the PCSSs based on SiC substrates are compared in Table 1. Ma et al. [10] reported a lateral-type PCSS based on HPSI 4H-SiC with a load resistance of 50-Ω. It achieved a minimum on-state resistance of 1.5 Ω with the optical energy of 5.5 mJ. The device conducted the output current of 450 A at a bias voltage of 26 kV.

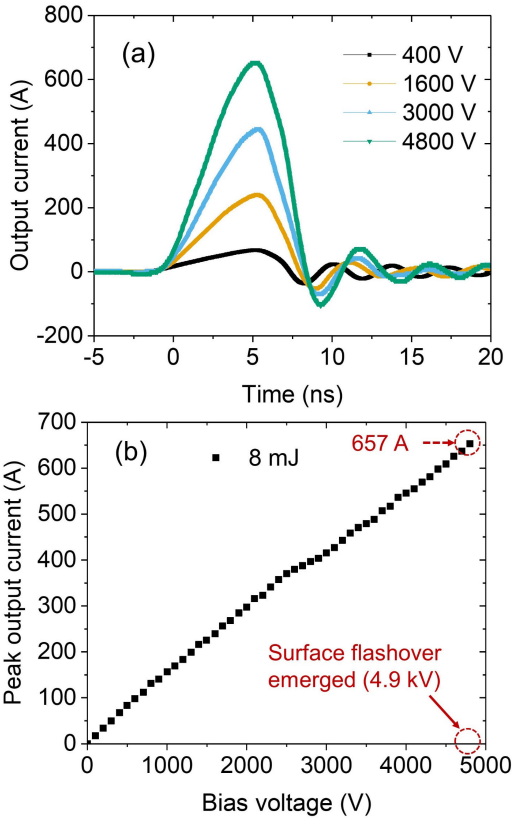

FIGURE 9. (a) Output current waveforms of the PCSS with a 0.05-Ω current viewing resistor under various bias voltages and (b) Peak output current of the PCSS with a load resistance of 0.05-Ω versus bias voltage at the optical energy of 8 mJ.

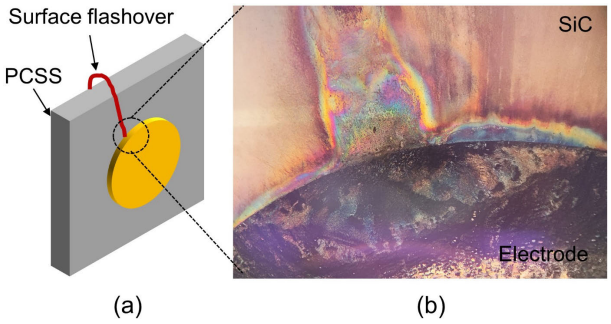

FIGURE 10. (a) Diagram of the PCSS breakdown phenomena by surface flashover (b) Optical microscope image of the damaged PCSS area after the surface flashover.

Collier et al. [17] reported that a vertical-type PCSS based on VCSI 6H-SiC based PCSS with a load resistance of 20-Ω demonstrated a minimum on-state resistance of 5.6 Ω with the optical energy of 31.9 mJ and an output current of 591 A

$$I_{N+1} = \frac{V_N - I_N\left(R_N(1 + \frac{C_{PCSS}}{C_c} - 2\frac{L_{CVR}C_{PCSS}}{(\Delta t)^2}) + R_{CVR}\right) - I_{N-1}\left(R_N(\frac{L_{CVR}C_{PCSS}}{(\Delta t)^2} - C_{PCSS}\frac{R_{CVR}}{2\Delta t}) - \frac{L_{CVR}}{2\Delta t}\right)}{R_N\left(\frac{L_{CVR}C_{PCSS}}{(\Delta t)^2} + C_{PCSS}\frac{R_{CVR}}{2\Delta t}) + \frac{L_{CVR}}{2\Delta t}\right)}. \quad (7)$$

TABLE 1. Performances of SiC-based PCSSs with various load resistances.

Ref.	Illumination type (structure)	Minimum on-state resistance (Ω)	Maximum switching current (A)	Optical energy (mJ)	Load res. (Ω)
[10]	Front (Lateral)	1.5	450	5.5	50
[17]	Front (Vertical)	5.6	591	31.9	20
[18]	Front (Vertical)	7.5	840	65	0.05
[24]	Side (Vertical)	0.66	1500	35.4	10.2
[25]	Front (Lateral)	<1	84	10.5	50
This work	Side (Vertical)	0.27	657	8	0.05

at a bias voltage of 18 kV. Cao et al. [18] reported that a vertical-type PCSS based on VCSI 4H-SiC with a 0.05-Ω CVR exhibited a minimum on-state resistance of 7.5 Ω with the optical energy of 65 mJ and output current of 840 A at the bias voltage of 12 kV. Sullivan [24] reported that a vertical-type PCSS based on VCSI 6H-SiC with a load resistance of 10.2-Ω achieved a minimum on-state resistance of 0.66 Ω under the optical energy of 35.4 mJ and the output current of 1500 A at a bias voltage of 17 kV. Xiao et al. [25] reported that a lateral-type PCSS based on HPSI 4H-SiC with a load resistance of 50-Ω achieved a minimum on-state resistance less than 1 Ω with the optical energy of 10.5 mJ. The output current was 84 A at a bias voltage of 6 kV. While the PCSSs with load resistances lower than 50-Ω achieved high current switching performances, the minimum on-state resistances, which were calculated using the output current at the CVR, were not clearly separated with the reactance. The transient analysis of the side-illuminated HPSI 4H-SiC based PCSS with load resistances of 50-Ω and 0.05-Ω exhibited the precise on-state resistance of 0.27 Ω. The maximum switching current capability of 657 A was demonstrated with a 0.05-Ω load under low optical illumination energy of 8 mJ.

IV. CONCLUSION

The output characteristics of vertical-type PCSS based on HPSI 4H-SiC was investigated using side-illumination with load resistances of 50-Ω and 0.05-Ω. When the PCSS was characterized with 50-Ω load, R_{eq} was inversely proportional to the optical energy, and t_{peak} showed similar values at various optical energies. On the other hand, the R_{eq} measured with a 0.05-Ω CVR exhibited saturating behavior and t_{peak} was found to depend on the optical energy, which is affected by the induced current at the inductance of the CVR. The current oscillation was caused by the natural response of the series RLC circuit with R_{CVR}, L_{CVR}, and C_{PCSS}. The PCSS in linear mode achieved a minimum R_{PCSS} of 0.27 Ω at the optical energy of 8 mJ and a maximum output current of 657 A at the bias voltage of 4.8 kV. Surface flashover was observed and was identified in the transient current pulse. The randomly occurring secondary pulses exhibited similar peak current and FWHM values.

REFERENCES

[1] L. Pecastaing, A. S. De Ferron, V. Couderc, B. M. Shalaby, R. Negrier, M. Lalande, J. Andrieu, and V. Bertrand, "A pulsed modulator combined with very high PRF photoconductive switches to build a self-scanning UWB radiation source," *IEEE Trans. Plasma Sci.*, vol. 44, no. 10, pp. 1894–1901, Oct. 2016, doi: 10.1109/TPS.2016.2547279.

[2] L. Hu, J. Su, R. Qiu, and X. Fang, "Ultra-wideband microwave generation using a low-energy-triggered bulk gallium arsenide avalanche semiconductor switch with ultrafast switching," *IEEE Trans. Electron Devices*, vol. 65, no. 4, pp. 1308–1313, Apr. 2018, doi: 10.1109/TED.2018.2802642.

[3] Q. Wu, Y. Zhao, T. Xun, H. Yang, and W. Huang, "Initial test of opto-electronic high power microwave generation from 6H-SiC photoconductive switch," *IEEE Electron Device Lett.*, vol. 40, no. 7, pp. 1167–1170, Jul. 2019, doi: 10.1109/LED.2019.2918954.

[4] C. Luan, J. Zhao, L. Xiao, Q. Yang, X. Ma, and H. Li, "All solid-state electromagnetic pulse simulator based on the 4H-SiC photoconductive semiconductor switch," *Rev. Sci. Instrum.*, vol. 91, no. 1, Jan. 2020, Art. no. 014701, doi: 10.1063/1.5128450.

[5] Y. Shen, W. Wang, Y. Liu, L. Xia, H. Zhang, H. Pan, J. Zhu, J. Shi, L. Zhang, and J. Deng, "A compact 300 kV solid-state high-voltage nanosecond generator for dielectric wall accelerator," *Rev. Sci. Instrum.*, vol. 86, no. 5, pp. 5–9, May 2015, doi: 10.1063/1.4921396.

[6] G. M. Loubriel, F. J. Zutavern, A. Mar, H. P. Hjalmarson, A. G. Baca, M. W. O'Malley, W. D. Helegeson, R. A. Falk, and D. J. Brown, "Longevity of optically activated, high gain GaAs photoconductive semiconductor switches," *IEEE Trans. Plasma Sci.*, vol. 26, no. 5, pp. 1393–1402, Oct. 1998, doi: 10.1109/27.736024.

[7] F. Davanloo, R. Dussart, K. J. Koivusaari, C. B. Collins, and F. J. Agee, "Photoconductive switch enhancements and lifetime studies for use in stacked Blumlein pulsers," *IEEE Trans. Plasma Sci.*, vol. 28, no. 5, pp. 1500–1506, Oct. 2000, doi: 10.1109/27.901222.

[8] M. Xun, D. Jianjun, L. Hongwei, Y. Jianqiang, L. Jinfeng, W. Bing, Q. Yanling, H. Wenhui, W. Lingyun, J. Pin, and L. Hongtao, "Development of all-solid-state flash X-ray generator with photoconductive semiconductor switches," *Rev. Sci. Instrum.*, vol. 85, no. 9, Sep. 2014, Art. no. 093307, doi: 10.1063/1.4895829.

[9] W. Shi and Z. Fu, "2-kV and 1.5-kA semi-insulating GaAs photoconductive semiconductor switch," *IEEE Electron Device Lett.*, vol. 34, no. 1, pp. 93–95, Jan. 2013, doi: 10.1109/LED.2012.2226558.

[10] C. Ma, W. Shi, M. Li, H. Gui, N. Hao, and P. Xue, "Impact of current filaments on the material and output characteristics of GaAs photoconductive switches," *IEEE Trans. Electron Devices*, vol. 61, no. 7, pp. 2432–2436, Jul. 2014, doi: 10.1109/TED.2014.2323052.

[11] D. Mauch, C. White, D. Thomas, A. Neuber, and J. Dickens, "Overview of high voltage 4H-SiC photoconductive semiconductor switch efforts at Texas tech university," in *Proc. IEEE Int. Power Modulator High Voltage Conf. (IPMHVC)*, Jun. 2014, pp. 23–26, doi: 10.1109/IPMHVC.2014.7287198.

[12] D. Mauch, W. Sullivan, A. Bullick, A. Neuber, and J. Dickens, "High power lateral silicon carbide photoconductive semiconductor switches and investigation of degradation mechanisms," *IEEE Trans. Plasma Sci.*, vol. 43, no. 6, pp. 2021–2031, Jun. 2015, doi: 10.1109/TPS.2015.2424154.

[13] Q. Wu, T. Xun, Y. Zhao, H. Yang, and W. Huang, "The test of a high-power, semi-insulating, linear-mode, vertical 6H-SiC PCSS," *IEEE Trans. Electron Devices*, vol. 66, no. 4, pp. 1837–1842, Apr. 2019, doi: 10.1109/TED.2019.2901065.

[14] J.-W.-B. Bragg, W. W. Sullivan, D. Mauch, A. A. Neuber, and J. C. Dickens, "All solid-state high power microwave source with high repetition frequency," *Rev. Sci. Instrum.*, vol. 84, no. 5, May 2013, Art. no. 054703, doi: 10.1063/1.4804196.

[15] M. S. Nikoo, A. Jafari, R. Van Erp, and E. Matioli, "Kilowatt-range picosecond switching based on microplasma devices," *IEEE Electron Device Lett.*, vol. 42, no. 5, pp. 767–770, May 2021, doi: 10.1109/LED.2021.3068732.
[16] M. G. Mazarakis et al., "High-current linear transformer driver development at Sandia National Laboratories," *IEEE Trans. Plasma Sci.*, vol. 38, no. 4, pp. 704–713, Apr. 2010, doi: 10.1109/TPS.2009.2035318.
[17] L. Collier, J. Dickens, J. Mankowski, and A. Neuber, "Performance analysis of an all solid-state linear transformer driver," *IEEE Trans. Plasma Sci.*, vol. 45, no. 7, pp. 1755–1761, Jul. 2017, doi: 10.1109/TPS.2017.2712361.
[18] P. Cao, W. Huang, H. Guo, and Y. Zhang, "Performance of a vertical 4H-SiC photoconductive switch with AZO transparent conductive window and silver mirror reflector," *IEEE Trans. Electron Devices*, vol. 65, no. 5, pp. 2047–2051, May 2018, doi: 10.1109/TED.2018.2815634.
[19] W.-W. Han, W. Huang, S.-Y. Zhuo, J. Xin, X.-C. Liu, E.-W. Shi, Y.-F. Zhang, P.-H. Cao, Y.-T. Wang, H. Guo, and Y.-M. Zhang, "A new method of accurately measuring photoconductive performance of 4H-SiC photoconductive switches," *IEEE Electron Device Lett.*, vol. 40, no. 2, pp. 271–274, Feb. 2019, doi: 10.1109/LED.2018.2885787.
[20] Y. Zhao, Q. Wu, T. Xun, L. Wang, and H. Yang, "A scalable, general purpose circuit model for vanadium compensated, semi-insulating, vertical 6H-SiC PCSS," *IEEE Trans. Circuits Syst. II, Exp. Briefs*, vol. 68, no. 3, pp. 988–992, Mar. 2021, doi: 10.1109/TCSII.2020.3021831.
[21] X. Chu, J. Liu, T. Xun, L. Wang, H. Yang, J. He, and J. Zhang, "MHz repetition frequency, hundreds kilowatt, and sub-nanosecond agile pulse generation based on linear 4H-SiC photoconductive semiconductor," *IEEE Trans. Electron Devices*, vol. 69, no. 2, pp. 597–603, Feb. 2022, doi: 10.1109/TED.2021.3138950.
[22] P. H. Choi, Y. P. Kim, M.-S. Kim, J. Ryu, S.-H. Baek, S.-M. Hong, S. Lee, and J.-H. Jang, "Side-illuminated photoconductive semiconductor switch based on high purity semi-insulating 4H-SiC," *IEEE Trans. Electron Devices*, vol. 68, no. 12, pp. 6216–6221, Dec. 2021, doi: 10.1109/TED.2021.3117535.
[23] C. K. Alexander and M. N. Sadiku, *Fundamentals of Electric Circuits*. Boston, MA, USA: McGraw-Hill, 2007.
[24] J. S. Sullivan, "High power operation of a nitrogen doped, vanadium compensated, 6H-SiC extrinsic photoconductive switch," *Appl. Phys. Lett.*, vol. 104, no. 17, pp. 2–6, May 2014, doi: 10.1063/1.4875258.
[25] L. Xiao, X. Yang, P. Duan, H. Xu, X. Chen, X. Hu, Y. Peng, and X. Xu, "Effect of electron avalanche breakdown on a high-purity semi-insulating 4H-SiC photoconductive semiconductor switch under intrinsic absorption," *Appl. Opt.*, vol. 57, no. 11, p. 2804, Apr. 2018, doi: 10.1364/ao.57.002804.

PYEUNG HWI CHOI received the B.S. degree from the School of Electrical Engineering and Computer Science, Gwangju Institute of Science and Technology (GIST), Gwangju, South Korea, in 2017, where he is currently pursuing the Ph.D. degree. His research interest includes photoconductive semiconductor switch (PCSS).

YONG PYO KIM received the M.S. degree from the School of Electrical Engineering and Computer Science, Gwangju Institute of Science and Technology (GIST), Gwangju, South Korea, in 2016, where he is currently pursuing the Ph.D. degree. His research interest includes photoconductive semiconductor switch.

MIN-SEONG KIM, photograph and biography not available at the time of publication.

JIHEON RYU, photograph and biography not available at the time of publication.

SUNG-HYUN BAEK, photograph and biography not available at the time of publication.

SUNG-MIN HONG (Senior Member, IEEE) received the B.S. degree in electrical engineering and the Ph.D. degree in electrical engineering and computer science from Seoul National University, Seoul, South Korea, in 2001 and 2007, respectively. He is currently an Associate Professor with the School of Electrical Engineering and Computer Science, Gwangju Institute of Science and Technology, Gwangju, South Korea. His main research interest includes physics-based device modeling.

SUNGBAE LEE received the B.S. and M.S. degrees in physics from Yonsei University, Seoul, South Korea, in 1998 and 2000, respectively, and the Ph.D. degree in physics from Rice University, Houston, TX, USA, in 2007. He is currently an Assistant Professor with the Department of Physics and Photon Science, Gwangju Institute of Science and Technology, Gwangju, South Korea. His main research interests include electron transports in novel materials and their applications.

JAE-HYUNG JANG (Senior Member, IEEE) received the B.S. and M.S. degrees in electrical engineering from Seoul National University, Seoul, South Korea, in 1993 and 1995, respectively, and the Ph.D. degree in electrical and computer engineering from the University of Illinois at Urbana–Champaign, Urbana, in 2002. He is currently a Professor and an Associate Dean at the Graduate School, the Chair at the School of Energy Engineering, Korea Institute of Energy Technology (KENTECH). Before joining KENTECH, he had been a Professor of electrical engineering and computer science, Gwangju Institute of Science and Technology (GIST), Gwangju, since 2004. During his stay at GIST, he served as the Chair of electrical engineering and computer science, from 2019 to 2021, and the Director at the Research Institute of Solar Energy (RISE), from 2015 to 2019. He is also doing active research on active metamaterial devices for microwave and THz applications. He is a Committee Member of IEEE Compound Semiconductor Devices and Circuit Division, a member of the Board of Directors at Korea Photovoltaics Society. His research interests include InP optoelectronic devices, SiC and GaN-based electron devices, GaAs, and CIGS-based thin-film solar cells.